Nanosized TiO2 is internalized by dorsal root ganglion cells and causes damage via apoptosis

Title: Nanosized TiO_2 is internalized by dorsal root ganglion cells and causes damage via apoptosis

Author names and affiliations:

Jessica Erriquez [a] [1], Vera Bolis [b], Silvia Morel [a], Ivana Fenoglio [b] [c], Bice Fubini [b] [c], Pierluigi Quagliotto [b], Carla Distasi [a] *

[a] Dipartimento di Scienze del Farmaco, Università del Piemonte Orientale "A. Avogadro", Largo Donegani 2, 28100, Novara, Italy.

[b] Dept. Chemistry, Interdepartmental Center for Nanostructured Interfaces and Surfaces (NIS), University of Torino, Italy

[c] ''G. Scansetti'' Interdepartmental Centre for Studies on Asbestos and other Toxic Particulates, University of Torino, Italy

[1] present address: Laboratory of Cancer Genetics, Fondazione del Piemonte per l'Oncologia (FPO)– Istituto di Ricovero e Cura a Carattere Scientifico (IRCCS), Candiolo, Italy

*** Corresponding author:**

Carla Distasi, Dipartimento di Scienze del Farmaco, Università del Piemonte Orientale "A. Avogadro", Largo Donegani 2, 28100, Novara, Italy. Phone: +39 (0) 321375810 e-mail: carla.distasi@pharm.unipmn.it

conflict of interest statement: None of the authors have any conflict to declare related to the study.

financial support information: Regione Piemonte CIPE 2006 Project: "Nanoparticles. From Their Impact on the Environment and Human Health to Safer Production and Usage (NANOSAFE)" coordinated by Bice Fubini.

abstract word count: 149
complete manuscript word count: XXX
number of references: XXX
number of figures: 6

Abstract

Titanium dioxide (TiO_2) is widely used as ingredient in several products in the nanoform. TiO_2-Nanoparticles (NPs) are also currently studied for different medical applications. A large debate exists on possible adverse health effects related to their exposure. While there are some evidences of toxic effects on the central nervous system, the effect TiO_2-NPs on peripheral neurons has been poorly explored. In this study we investigated the effects TiO_2-NPs on Dorsal Root Ganglion (DRG) sensory neurons and satellite glial cells that may be reached by nanoparticles from the bloodstream. We found that TiO_2-NPs are internalized in DRG cells and induce apoptosis in a dose dependent manner in both types of cells, ROS production and changes in expression of proinflammatory cytokine IL-1β. Furthermore, we found that the axonal retrograde transport is altered in neurons upon exposure to TiO_2-NPs. Overall, the results indicate a potential neurotoxic effect of TiO_2-NPs on DRG cells.

Key words

titanium dioxide, nanoparticles, dorsal root ganglion, apoptosis, ROS, IL-1β, axonal transport

Background

Despite the increased presence of nanosized TiO_2 particles (TiO_2-NPs) in consumer products about a general consensus on their effects on human health has not been reached yet. While a wide literature may be found on the effect of TiO_2 on central nervous system [1-11] almost nothing is known about their impact on peripheral sensory neurons. This study is aimed to fill in part this gap by investigating the cytotoxic effects of low doses of TiO_2-NPs on primary cultures of dorsal root ganglia (DRG). DRG confine the cell bodies of primary somatic afferent neurons that transmit sensory information from the periphery into the central nervous system. Within the ganglion, neuronal cell bodies are surrounded by satellite glial cells (SGCs), that play vital roles in sensory ganglia physiology.[12,13]

In principle sensory neurons can be achieved in vivo by the nanoparticles through two distinct pathways. The first is penetration through the skin. This way is certainly restricted in healthy skin but may not be negligible in the case in which pharmaceuticals, cosmetic products and sunscreens containing titanium dioxide are spread on broken or inflamed skin especially for long time of exposure.[14,15] Indeed nanoparticles can be internalized by the free sensory nerve endings of C- and Aδ-fibers that innervate the skin and reach the superficial layers of the epidermis. Nanoparticles taken up by endocytic mechanisms can be transported to the cell body and to the central terminals of neurons so that afferent sensory nerves can also serve as portals of entry to the central nervous system.

The second way by which TiO_2-NPs can reach sensory neurons is by blood circulation. TiO_2-NPs were indeed found in erythrocytes within the pulmonary capillaries of rat that inhaled aerosol containing 20 nm TiO_2-NPs [16] or in blood vessel of mice after intraperitoneal injection.[17] Moreover, TiO_2 NPs are promising materials for medical applications and are under investigation, for

example, for their anticancer properties and in the field of advanced imaging.[18,19] For many therapeutic or diagnostic applications in the nanomedicine, nanoparticles are to be injected intravenously. It is worth mentioning that DRG lack an efficient neurovascular barrier as they contain blood vessels which have no tight junctions and possess fenestrae [20] through which nanoparticles can pass. On the other hand, inside the ganglion a direct interaction of materials leaving the capillaries with neuronal plasma membrane is strongly limited by SGCs. Indeed these cells enwrap neuronal cells bodies and regulate the exchange of substances from the blood to the neurons: SGCs, together with macrophages, possess phagocytic activity and are actively involved in the clearance of cellular debris and exogenous material from peripheral nervous system.[13,21] Thus the first targets of cytotoxic effects of nanoparticles carried by blood circulation in the sensory ganglia are probably SGCs themselves.

In the present study we investigated if low-dose exposure to nanosized TiO_2 has pro-apoptotic effects in DRG neurons and SGCs, the uptake and the intracellular localization of nanoparticles and their influence on retrograde axonal transport, ROS production and expression of the proinflammatory cytokine IL-1β.

METHODS

TiO_2 nanoparticles

TiO_2-A/R (Aeroxide P25, Degussa-Evonik Goldschmidt, Frankfurt, Germany) and TiO_2-R (MT 500 B Rutile, LCM Trading, Milano, Italy) specimens are commercial samples kindly supplied by the companies; TiO_2-A specimen was synthesized ad hoc by sol gel technique as previously described

in Bolis et al.[22] The samples were fully characterized as previously described.[22] The main physico-chemical properties of the nanomaterials are listed in Table S1 (SM).

Preparation of FITC-TiO_2 labelled nanoparticles

Preparation of the label. In a three necked round bottom flask (50 ml), the fluorescein isothiocyanate (FITC) and ethanol were introduced under Argon and stirred, while the flask was carefully covered to avoid contact with light. After 10 minutes all material was dissolved and 3-aminopropyltriethoxysilane (APTS) was added by a syringe under continuous stirring. After 1 day, the reaction was complete and samples were taken to react the label with the titania particles (see below). The label was characterized by NMR and MS (see SM).

Labelling. The titania powder (2 grams) was introduced in a 500 ml three necked flask, and heated (150°C) overnight in an oven. The flask was closed with rubber stopper and degassed with Argon 3 times. Anhydrous ethanol (about 50 ml per gram of titania) was introduced and stirred under argon flux and stirring for 15 minutes.

1 ml of the solution of the label (see above) was diluted to 10 ml and an aliquot of this solution was taken, to have about 1:1 reactant to hydroxyl group ratio, based on the hydroxyl groups density at the titania surface. The fluorescent marker solution was dropped slowly into the titania suspension at room temperature under vigorous stirring. The reaction was stopped after 22 h. The suspension was transferred into several Falcon tubes and centrifuged at 4000 rpm for 10 minutes. The pellet was washed a few times with fresh dry ethanol until clear and not colored and dried in an oven at about 50°C overnight. The powder was stored into a brown container, to avoid contact with light.

Characterization of the fluorescent nanoparticles

Microcalorimetry. The enthalpy change associated with the adsorption of H_2O vapour on the investigated samples was measured at T = 30°C by means of a heat-flow microcalorimetry (Calvet C80, Setaram, France) connected to a high vacuum gas volumetric glass apparatus (residual pressure $p \leq 10^{-5}$ Torr).

ζ potential and hydrodynamic diameter. Dynamic Light Scattering and electrophoretic mobility of TiO_2 nanoparticle (TiO_2-NP) aggregates dispersed in solution (NaCl 1 mM for potential versus pH analysis: pH was varied from 2 to 10 by the addition of NaOH or HCl to appropriate concentrations) or in culture medium (pH 7.4) were measured at T = 25°C by employing the Zetasizer apparatus.

Turbidimetry. The sedimentation rate of nanoparticles dispersed in medium was determined by monitoring the optical absorbance (at 337 nm) as a function of time, during a time interval of 3 and 24 hours, by UV – vis spectrometer lambda 35 (Perkin Elmer & Co. GMBH, Überlingen, D).

DRG cell cultures

Cell culture protocols have been described in detail previously.[23] Briefly, dorsal root ganglia were dissected from 7 day-old chick embryos. Dissociated cells were counted and 150 µl of cell suspension containing nearly 18000 cells was plated in 24-well plates or, for DAPI/NeuroTrace staining and time lapse video microscopy experiments, in the middle of area of a glass coverslip coated with poly-D-lysine (100 µg/ml) and laminin (2 µg/cm^2). Cells were incubated for 1-2 hours at 37°C in a humidified atmosphere containing 5% of CO_2 to allow cells to adhere to the substrate and the plastic petri dish containing the coverslip was filled with serum free N2 medium.

Viability assay

Cell viability was evaluated using two fluorescent dye-based assays: deoxynucleotidyl transferase dUTP nick end labeling (TUNEL) staining for detecting DNA fragmentation, and a simultaneous staining with 4',6-diamidino-2-phenylindole (DAPI) and NeuroTrace to distinguish if the cells undergoing apoptotic nuclear fragmentation are neurons or SGCs. After 24 hours of culture, DRG cells were washed twice and exposed in the dark for 24 hours at 37°C to TiO_2-NPs freshly dispersed in cell culture medium as previously described.[22]

TUNEL staining. Cells were fixed in 4% paraformaldehyde (PFA) in Phosphate-buffered saline (PBS) and stained by using the APO-BRdU TUNEL assay kit (Invitrogen). Final detection of BrdU incorporation at DNA break sites was achieved through an Alexa Fluor 488-labeled anti-BrdU antibody. Nuclei were counterstained with propidium iodide (PI). Alexa Fluor 488- and PI-fluorescent images were collected with a confocal microscope (TCS SP2, Leica), using an excitation wavelength of 488 nm and 514 nm for Alexa Fluor 488 and PI respectively, and detection was in the range of 500-530 nm for Alexa Fluor 488 and of 600-630 nm for PI. TUNEL-positive nuclei were counted in 5 randomly chosen 20x microscope fields per well. An experiment consisted of measuring the percentage of apoptotic cells, calculated as the number of TUNEL-positive cells/number of total cells×100, in duplicate wells.

DAPI/NeuroTrace staining. NeuroTrace fluorescent Nissl stain (Invitrogen) is successfully used to identify DRG neurons.[24] After fixation (PFA; 4%), cultured DRG cells were rinsed in PBS alone, in PBS plus 0.1% Triton X-100 and incubated with NeuroTrace at 1:200 dilution for 20 min. Cells were extensively washed with PBS, incubated with DAPI (0.5 μg/ml) for 15 min and then washed with PBS. Images were acquired by means of an inverted microscope (Eclipse TE 300, Nikon) equipped with a monochromator (Polychrome IV, T.I.L.L. Photonics, Germany) and a digital camera (SensiCam, PCO, Gemany). Dye was excited at a wavelength of 500 nm and 358 nm for NeuroTrace

Green and DAPI respectively. Images in grayscale were converted to green-colored (NeuroTrace) images or blue-colored (DAPI) images. The number of fluorescently labeled cells was counted using NHI ImageJ software.

Uptake and intracellular localization of FITC-labeled TiO_2-NPs

Cells were incubated for 2 hours or for 24 hours at 37°C in culture medium with 5 μg/ml of FITC-TiO_2-NPs. To determine whether lysosomes and mitochondria were internalization sites for the nanoparticles, live cells were then incubated with the fluorescent dyes LysoTracker Red (50 nM, 1 minute and 30 seconds, Invitrogen) or MitoTracker Orange CMTMRos (100 μM, 30 minutes, Invitrogen). Cells were washed with PBS and fixed (PFA, 1%) in PBS for 15 min at -20°C. The fluorescence signals were visualized using confocal microscopy. The laser excitation wavelengths used were Exc = 488 nm for FITC, Em = 543 nm for MitoTracker and LysoTracker; detection was in the range of 490-505 nm for FITC and of 600-630 nm for MitoTracker and LysoTracker. Co-localizations of nanoparticles with LysoTracker and MitoTracker probes appear yellow/orange in merged images.

Endocytic labelling and time lapse video microscopy

Cells were incubated in culture medium supplemented with 0.5 mM 8-Hydroxypyrene-1,3,6-trisulfonic acid (HPTS) for 20-24 hr. Glass coverslips were transferred in a live cell imaging chamber (Bioptechs, USA) and mounted on an inverted microscope (Eclipse TE 300, Nikon, Japan). Experiments were performed at a chamber temperature of 37°C and labeled cells were bathed in Tyrode's solution of the following composition (mM): NaCl, 154; KCl, 4; $CaCl_2$, 2; $MgCl_2$,1; N-(2-

Hydroxyethyl)-piperazine-N-ethanesulfonic acid (HEPES), 5; glucose, 5.5; pH 7.4 (adjusted with NaOH). Visualization of HPTS containing organelles was achieved exciting the dye alternatively at 415 nm and 450 nm for 200 ms, at a frequency of 0.3–0.5 Hz by means of a monochromator (Polychrome IV, T.I.L.L. Photonics GmbH, Germany). Images were recorded with a digital camera (SensiCam, PCO, Germany) and stored on a computer. Organelles trajectory was determined as the time sequence of the centroid position of the organelle recorded exciting the dye at 415 nm using a custom made software written by SITEM, Italy. Instantaneous retrograde axonal organelle speed (μm/min) was calculated from displacement between two subsequent positions for all images in a time series composed of at least seven frames.

Detection of Reactive Oxygen Species (ROS) generated by TiO_2-NPs

ROS production was detected using the CellROX Deep Red (Life Technologies) staining, a fixable and cell-permeable dye that exhibit fluorescence upon oxidation. After 24 hours of culture, DRG cells were washed twice, exposed in the dark for 4 hours at 37°C to TiO_2-NPs alone (5 μm/ml) or TiO_2-NPs plus the antioxidant N-acetylcysteine (NAC) 5 mM or H_2O_2 alone (20 μM). Cells were incubated for additional 30 min with CellROX Deep Red (5 μM), washed and fixed in 4% PFA in PBS. Nuclei were counterstained with DAPI. Images were collected at confocal microscope (excitation wavelength of 644 nm and 358 nm for CellROX and DAPI respectively; detection in the range of 655 nm for CellROX and of 461 nm for DAPI). CellROX positive cells were counted in 5 randomly chosen 20x microscope fields per well.

Quantitative PCR

Total cellular RNA was isolated using the SV Total RNA Isolation kit (Promega, Fitchburg, WI, USA) following the manufacturer's instructions. RNAs were then quantified and inspected by Bioanalyzer (Agilent Technologies, Waldbrom, Germany) analysis. To quantify the expression levels of chicken Interleukin 1β (GenBank accession no. NM_204524) encoding genes, equal amounts of cDNA were synthesized using the Moloney murine leukemia reverse transcriptase (Promega, Madison, WI) and mixed with SsoFast EvaGreen Supermix (Bio-Rad, Hercules, CA, USA) and each of the respective forward and reverse primers. Quantitative real-time PCR was done on CFx96 Real Time System thermal cycler (Bio-Rad, Hercules, CA). Each target gene expression was evaluated using a relative quantification approach ($2^{-\Delta\Delta CT}$ method), with chicken Actin β (GenBank accession no. NM_205518) as an internal reference. Primer sets used are as follows:

ch_IL-1b for	5'-TGGGCATCAAGGGCTACA-3'
ch_IL-1b rev	5'-TCGGGTTGGTTGGTGATG-3'
ch_actin-b for	5'-CACAGATCATGTTTGAGACCTT-3'
ch_actin-b rev	5'-CATCACAATACCAGTGGTACG-3'

Sample size and statistical analysis of experiments

TUNEL staining, DAPI/NeuroTrace staining, CellROX staining, intracellular localization of FITC-labeled TiO_2-NPs and qPCR experiments were repeated three times at least in duplicate on separate days on separate primary cultures. Endocytic labelling and time lapse video microscopy experiments were done on 14 separated days on separate primary cultures.

Data are presented as the mean values ± SEM. Student's t test or one-way ANOVA followed by a statistical test for multiple comparisons (OriginPro, Tukey's test) were applied to compare experimental treatments. A probability level of < 0.05 was considered statistically significant.

Results

Synthesis and characterization of TiO_2 fluorescent nanoparticles

Functionalization was aimed at using the fluorescence signal as "live tracer" of the fate of TiO_2-NPs, in order to assess their interference with biological systems and the possible toxicity. The method of functionalization was chosen in order to obtain a high fluorescence signal, consistent with the minimum disturbance of the surface of nanoparticles themselves.[25]

The linkage of FITC to the surface of a nanoparticle may dramatically modify the charge of the surface and, in turn, the hydrodynamic size of the particles and the stability of the suspension of the nanomaterial in aqueous solution. In the present case, the effect of the label on the surface charge has been evaluated indirectly by measuring the ζ potential as function of pH of the materials suspended in water (see SM). In the case of TiO_2-A/R (Fig. S1, A) (see SM) the ζ potential curve obtained on the labeled nanoparticles does not significantly differs from those of the pristine material, while for TiO_2-A (Fig. S1, B) and for TiO_2-R (Fig. S1, C) a shift of the curve toward more acidic pH, due to the contribution of the acidic carboxylic and phenol groups on the label, is observed suggesting a higher abundance of labels at the surface for the latter specimen. In any case a shift of the curves toward basic pH, indicative of a possible presence of free amino groups deriving from an incomplete reaction between spacer and label, was observed.

To further investigate the effect of labeling on the surface properties of the nanoparticles the hydrophilic degree of the labeled and pristine TiO_2-A/R was evaluated by means of microcalorimetric measurement using water vapor as probe molecule (see SM). The amount of water taken up by FITC-TiO_2-A/R was significantly lower than that taken up by TiO_2-A/R (6.8 μmol/m^2 versus 10.7 μmol/m^2 at p_{H_2O} ≈ 6 Torr) as well as the enthalpy associated to adsorption.

This was expected due to the presence of the organic labels covalently linked to the surface. Overall, the labeled titania appear hydrophilic similarly to the pristine one.

Characterization of fluorescent TiO_2-NPs in cell media

When nanoparticles came in contact with the cell media the neutral pH, the ionic strength and the presence of molecules, particularly proteins, that adsorb at the surface largely affect the ζ potential of particles and their agglomeration degree. Agglomeration is known to be an important parameter that modulates the cell response to nanomaterials.[26] In table S2 (see SM) the ζ potential and the hydrodynamic size of the materials dispersed in simplified cell medium DMEM/F-12 supplemented only with BSA (2 mg/ml) (the protein mainly present in culture medium) is reported. As previously reported by some of us[27] the formation of large agglomerates with sizes ranging from hundreds of nanometers to micrometers is observed for all samples as a consequence of the high ionic strength and of the neutral pH of the solutions. The functionalization slightly affects both ζ potential and the hydrodynamic size of the particles, suggesting that, the functionalized samples maintain the same properties of original specimens.

To ensure the stability during the time of fluorescent sample dispersions, turbidimetry experiments were set up. After dispersion of samples in culture medium, they were monitored using a spectrophotometer for 3 hours and after 24 hours: all dispersions resulted stable up to 24 hours (at 92-100%, data not shown).

TiO_2-NPs exposure alters DRG cell morphology

Figure 1a shows the appearance of primary cultures established from DRG of chicken embryos when cultivated for 2 days (DIV2). In a previous study Erriquez et al.[23] have shown that, under exactly the same conditions as those used here, the culture contain almost exclusively (about 97%) a mixture of different neural cells types: most (about 75%) of DRG cells are SGCs that exhibit a flattened, polygonal morphology, whereas the remaining cells are neurons with long neurites emerging from oval or round phase-bright cell bodies (figure 1a). In figure 1b and 1c are shown DRG cells that, after DIV1, have been incubated for another day with 0.5 µg/ml or 5.0 µg/ml of TiO_2-A/R NP dispersions, respectively. Most cells are still adherent but they show severe morphological alterations, such as thinner neurites, changes of cell volume and shrinkage, that are indicative of a loss of cell viability.

Pro-apoptotic effects and intracellular fate of TiO_2-A/R-NPs

In a previous study we have shown a cytotoxic effect of TiO_2-A/R-NPs on primary DRG cultures by quantifying the fraction of nuclei with fragmented DNA in cells exposed for 24 hours to NP dispersions.[22] However, neither dose-dependent effects nor specific cytotoxic effects of TiO_2-A/R-NPs on neuronal versus glial cells were evaluated. To address these issues, DRG cultures after DIV1 were exposed for 24 hours to two increasing doses of TiO_2-A/R-NPs, 0.5 µg/ml or 5.0 µg/ml, and then processed, together with parallel untreated cultures, for TUNEL analysis. In figure 2a are shown representative images of control and treated cells double labeled with the red fluorescent nuclear dye propidium iodide and the green fluorescent TUNEL staining. Exposure to TiO_2-A/R-NPs induced an increase in the number of TUNEL-positive nuclei. The figure 2b represents the results of the quantitative analysis: the mean percentage of TUNEL-positive nuclei in control condition was 8.2 ± 2.7; in the presence of 0.5 µg/ml of TiO_2-A/R this percentage was significantly higher

(24.6 ± 6.0%, $p < 0.05$) and a still higher percentage was observed in the presence of 5.0 µg/ml (39.6 ± 8.2%, $p < 0.01$).

In order to investigate the cell types undergoing cell death upon TiO_2-A/R-NPs exposure, we evaluated the nuclear fragmentation in cells double stained with the nuclear dye DAPI and the neuron specific marker NeuroTrace green fluorescent Nissl stain. Results are illustrated in figure 3. Double DAPI-Nissl stain revealed the characteristic features of DRG neurons, including an eccentric nucleus with one or two nucleoli and the presence of Nissl-positive material in the cytoplasm (panel a, b, c and e). SGCs exhibit a more elliptical nucleus with Nissl-positive clumps (panel a, b, c and d). Examples of a neuron and of a glial cell displaying a fragmented nucleus are shown by arrows in panels 3d and 3e, respectively. The ratio between SGCs and neurons did not change significantly upon treatments (5.3 ± 0.8 in control condition compared to 4.7 ± 0.2 and 3.9 ± 0.4 in the presence of 0.5 µg/ml or 5.0 µg/ml TiO_2-A/R-NPs, respectively), while this was not the case for the percentage of apoptotic cells. The mean percentages obtained for all apoptotic DRG cells in untreated cultures (CTRL) and in cultures exposed for 24 hours to increasing doses of TiO_2-A/R-NPs are depicted in the figure 3f, while those of apoptotic SGCs alone and those of apoptotic neurons alone are shown in panels 3g and 3h respectively. In all cases we observed a significant dose-dependent increase of cell death. These results indicate that TiO_2-A/R-NPs exhibit a similar toxicity towards neurons and SGCs.

To investigate if TiO_2-NPs were internalized by neurons and SGCs and their localization into the cell soma and along the axons, in a first series of experiments cultures were exposed for 2 hours at 37°C to FITC-TiO_2-A/R-NPs at a density of 0.5 µg/ml and then incubated with LysoTracker Red, a fluorescent dye for labeling acidic organelles. Figure $4a_2$ shows the intracellular localization of FITC-TiO_2-A/R in neurons: green fluorescence was confined to small round structures along neurites and in cell bodies. Figure $4a_3$ shows the LysoTracker Red positive organelles: many of

them have been found to colocalize with the internalized nanoparticles, as shown by the yellow areas in the overlay image of figure $4a_4$. A similar pattern of staining was observed in SGCs (figure $4b_2$-b_4). After 24 hours of incubation, as shown in the series of confocal sections acquired along the z-axis of a neuron (Figures $4c_1$-c_4, bottom to top), nanoparticles were extensively colocalized with many acidic vesicles present throughout the soma and the neurite.

To further clarify the intracellular distribution of nanoparticles, mitochondria in DRG cells treated with 5 μg/ml of fluorescent nanoparticles were stained with the fluorescent dye MitoTracker Orange CMTMRos. After 24 hours of exposure, nanoparticles colocalization with mitochondria was weak in neurons, although not completely absent, as showed in the series of confocal sections acquired along the z-axis of a neuron (figures $4d_1$-d_4). A more extensive colocalization was observed in SGCs body (figure $4e_2$-e_5).

In conclusion, our data demonstrate that TiO_2-A/R-NPs are extensively internalized into SGCs and sensory neurons mainly via endocytosis, and that most of them reside in acidic vesicles, lysosomes and to a lesser extent in mitochondria or in their proximity.

Effect of the crystalline phase on the toxicity and intracellular fate of TiO_2-NPs

Cytotoxic dose-dependent effects were also evaluated for two other pristine TiO_2-NPs, Rutile (TiO_2-R) and sol-gel Anatase (TiO_2-A). In the case of TiO_2-R, no induction of apoptosis, evaluated as percentage of TUNEL-positive cells, was observed with any of the two doses tested, 0.5 μg/ml or 5.0 μg/ml (SM, figure S3a). A significant effect was conversely obtained when cells were incubated with the higher dose of TiO_2-A nanoparticles (SM, figure S3b). We then investigated if differences exist in the intracellular distribution of FITC-TiO_2-R and FITC-TiO_2-A NP that can account for the

variation in the toxicity observed with the different polymorphs. Confocal microscopy analysis revealed an intracellular distribution profile very similar for all specimens studied (SM, figure S4).

TiO_2-A/R-NPs affect retrograde axonal transport

Retrograde axonal transport plays a fundamental role in the maintenance of neuronal function, plasticity, morphogenesis and survival. Several organelles, molecules and pathogens are targeted to the soma via retrograde transport. Moreover, alteration of axonal transport is a hallmark of several neurodegenerative diseases.[28,29] For these reasons we investigated if the retrograde axonal transport in DRG neurons is altered in cells exposed to TiO_2-A/R-NPs. To quantitatively study the axonal transport we used time lapse video-microscopy to follow the trajectories of endocytic vesicles labeled with the fluorescent membrane-impermeant HPTS vital dye, which is uptaked by the cells via endocytosis. Figure 5a and 5b illustrate an example of a trajectory traced by tracking the retrograde movement of a vesicle along the axon. Figure 5c a compares the mean speed v obtained tracking the motion of 53 retrograde vesicles from untreated neurons in different cultures and of 64 vesicles from neurons in parallel control cultures that were exposed overnight to 5 μg/ml TiO_2-A/R-NPs. These data reveal the ability of the nanoparticles to affect the retrograde transport of endocytic vesicles as their mean speed was significantly increased in their presence (v = 1.08 μm/s ± 0.07) compared with control (v = 0.84 μm/s ± 0.08, $p < 0.05$ t-test). On the other hand, no statistically significant difference was found in mean velocity between retrograde vesicles from neurons incubated with TiO_2-R-NPs (v = 1.04 μm/s ± 0.08, n = 59) and those from untreated neurons (v = 0.92 μm/s ± 0.07, n = 57, Figure 7d). The speed distributions obtained in the different experimental conditions are shown as histograms in panels 7 e-h: only the incubation of neurons with TiO_2-A/R-NPs alters the basic shape of the distribution.

TiO_2-A/R-NPs induce generation of ROS and increase IL-1β expression in DRG cells

To provide deeper insights into the mechanisms involved in TiO_2 NPs cellular toxicity, we assessed ROS production using the CellROX dye. The majority of the CellROX-traeted cells showed a diffuse cytoplasmic red staining when incubated with H_2O_2 (Figure 6a) and TiO_2-A/R-NPs. In addition, also NPs appeared red stained, as shown in images acquired with confocal reflection microscopy and merged with CellROX-DAPI images. Notably, the antioxidant NAC inhibited the fluorescence signal in cells by not in NPs that still appeared red. Finally, TiO2-R-NPs did not induce ROS generation in DRG cells. The mean percentage of CellROX-positive cells are shown in the figure 6b.

Upregulation of proinflammatory cytokines including IL-1β, a cytokine expressed in embryonic chicken DRG from early stages of developmentCIT2A, represents one of the earliest events observed in sensory nerves in response to neuronal injuryCIT2B. For these reasons we measured if TiO_2A/R-NPs can affect IL-1β expression at mRNA level. As shown in figure 6c, In cells incubated for 24 hours with 5 μM of TiO2-A/R-NPs the level of IL-1β mRNA increased significantly, suggesting that NPs triggered cytokine expression in DRG cells

Discussion

In embryonic and postnatal life, different types of neurons have and retain the ability to internalize material of various size, up to 1 μm.[30] Thus is not surprising that nanoparticles are in vitro rapidly internalized in DRG neurons via endocytic mechanisms as shown by their extensive colocalization with acidic vesicles as observed in the present study. Our data also demonstrate that the axonal transport, although altered in the presence of TiO_2-A/R, is not completely compromised: nanoparticles from periphery can be transported along the sensory fibers.

In this study we shown for the first time that TiO_2-A/R, which is internalized by endocytosis by SGCs, is toxic for these cells at low doses (0.5-5 µg/ml). Several experimental data that has been accumulated recently on the physiology of SGCs indicate that they are actively involved not only in many normal processes of the sensory ganglia, but that they also play an active role in the initiation and maintenance of pathologic dysfunctions such as neuropathic pain.[12,31] TiO_2-NPs can then interfere with the physiological functions of the sensory ganglia either through direct cytotoxic action on neurons or indirectly through damage to SGCs.

Nanosized TiO_2 in the anatase, rutile or mixed phase forms show a very different degree of acute toxicity. This disparity in toxicity levels is not due to different ways of handling by the cells, because our experiments indicate that the intracellular fate is the same for all the specimens investigated, but rather should be dependent to intrinsic differences in physico-chemical properties of the samples. In PC12 cells TiO_2-A/R was shown to be more toxic than anatase, while rutile did not induce apoptosis after 24 hours of incubation, although adverse effects may occur in a time-dependent manner.[32] Moreover, it should be noted that in DRG cells mixed phase and TiO_2-A-NPs induce pro-apoptotic effects at low doses. In many other cell types like macrophages,[33] lymphocytes,[34] keratinocytes,[35-37] neuroendocrine PC12 cells,[32,38] bronchial and lung cells,[39,40] TiO_2-NPs promote apoptosis at doses 20 to 100 times greater than those observed in our study.

However, the concentrations used in the present in vitro study are probably still high compared to the blood concentrations expected by exposure to doses that are realistic for humans. Several in vivo studies showed that TiO_2-NPs are poorly absorbed following inhalation, oral or dermal exposureCIT1A. On the other hand, biokinetic studies showed that TiO_2-NPs elimination from the body is a very slow process and over time nanoparticles are released from primary target organs and redistributed between organs and tissuesCIT1B, so that a low but continuous exposure can give a non negligible and toxic accumulation in neuronal cells.

Like others cells types,[5,32,39] in response to TiO_2-NPs exposure DRG cells generate reactive oxygen species. ROS are believed to produce oxidative stress,[41] the imbalance between cellular production of ROS and cell antioxidant defense mechanisms that can induce cell death. Nervous system is especially vulnerable to oxidative stress: despite the oxygen consumption is very high in neural tissue, the antioxidant activity is modest in comparison with other tissues. Moreover, neural cell membranes contain high levels of polyunsaturated fatty acid which are particularly susceptible to peroxidation and oxidative modification which can cause membrane rupture and alterations in the function of receptors, ion channels, and signaling molecules.[42] Notably, TiO_2-A/R-NPs but not R-NPs exposure induces ROS generation and apoptosis in DRG cells and these results strongly suggest that the enhancement of intracellular ROS levels is one of the key factors for TiO_2-NPs pro-apoptotic effect. Moreover, we observed that TiO_2-A/R-NPs also increases IL-1β expression, a cytokine that has been implicated as extracellular signal not only in the initiation of apoptosis in neurons and glial cells but also of several neurological and neurodegenerative deseases.CIT2B. It is noteworthy that in a variety of cell types, anatase TiO_2-NPs are significantly more potent than rutile in producing adverse biological effects.[1,35,38,43,44] On the other hand mixed anatase-rutile phase TiO_2-NPs like Aeroxide P25 was shown to elicit adverse effects larger than that of anatase specimens.[27] This was confirmed in our study where we also observed an order of increasing toxicity of the different polymorphs on DRG cells, anatase/rutile > anatase > rutile. Several physico-chemical properties may be related to the observed differences. The photocatalytic activity of TiO_2 has been shown to play a role in the toxicity of nanometric TiO_2 under illuminated conditions,[45] but it was also suggested to have a role in the absence of illumination.[43,46] Since these specimens exhibit a photocatalytic efficiency in the order anatase/rutile > anatase > rutile it may be one reason of the observed adverse effect. We cannot exclude, however, that the observed differences are related to the different surface area of the

samples since it has been recognized to be an important determinant of TiO_2 toxicity.[47,48] Oxidative stress is also a contributing factor to a number of neurodegenerative diseases,[49] which in many cases are associated with alterations in axonal transport. [28,29] Active transport along the axon is in fact a crucial process for neuronal function and survival as it provides molecules to the distal synapses, mitochondria for local energy supplies and neurotrophic and environmental signals from axon terminals to the cell soma. Thus our finding that in neurons exposed to TiO_2-A/R-NPs the retrograde axonal transport is significantly increased is outstanding because this alteration may have a serious impact on the function and life of sensory neurons. Notably, a similar effect was also observed in axons treated with 1-methyl-4-phenylpyridinium, a neurotoxin that induces Parkinson's disease symptoms, neuronal cell death and that alters the retrograde axonal transport through activation of caspase-3, a principal protease involved in neuronal apoptosis, and of protein kinase C.[50] We cannot exclude that the ability of TiO_2-A/R-NPs to increase the retrograde axonal transport is directly related to its pro-apoptotic effect in DRG cells but further experimental investigations are needed to confirm this hypothesis. Finally, the TiO_2 NPs adverse effects observed at cellular level in this study can also have crucial implications on nervous system development, not only during postnatal life but also in the course of embryonic life. Maternal exposure to different specimens of TiO_2 produce several modifications in many region in the brain of offspring, such as changes in gene expression, apoptosis, dopamine levels and neurobehavioral alterationsCIT1CCIT1D.

In conclusion, the neurotoxic effects observed in sensory neurons and SGCs imply that nanoparticles can potentially cause health risk, not only acutely but also in the long term, by triggering or aggravating neurodegenerative diseases.

References

1. Wang J, Chen C, Liu Y, Jiao F, Li W, Lao F et al. Potential neurological lesion after nasal instillation of TiO(2) nanoparticles in the anatase and rutile crystal phases. *Toxicol Lett* 2008;**183**:72-80.

2. Suh WH, Suslick KS, Stucky GD, Suh YH. Nanotechnology, nanotoxicology, and neuroscience. *Prog Neurobiol* 2009;**87**:133-170.

3. Simkó M, Mattsson MO. Risks from accidental exposures to engineered nanoparticles and neurological health effects: a critical review. *Part Fibre Toxicol* 2010;**7**:42.

4. Hu R, Gong X, Duan Y, Li N, Che Y, Cui Y et al. Neurotoxicological effects and the impairment of spatial recognition memory in mice caused by exposure to TiO2 nanoparticles. *Biomaterials* 2010;**31**:8043-8050.

5. Gramowski A, Flossdorf J, Bhattacharya K, Jonas L, Lantow M, Rahman Q et al. Nanoparticles induce changes of the electrical activity of neuronal networks on microelectrode array neurochips. *Environ Health Perspect* 2010;**118**:1363-1369.

6. Ma L, Liu J, Li N, Wang J, Duan Y, Yan J et al. Oxidative stress in the brain of mice caused by translocated nanoparticulate TiO2 delivered to the abdominal cavity. *Biomaterials*; 2013;**31**:p. 99-105.

7. Hu R, Zheng L, Zhang T, Gao G, Cui Y, Cheng Z et al. Molecular mechanism of hippocampal apoptosis of mice following exposure to titanium dioxide nanoparticles. *J Hazard Mater* 2011;**191**:32-40.

8. Gao X, Yin S, Tang M, Chen J, Yang Z, Zhang W et al. Effects of developmental exposure to TiO2 nanoparticles on synaptic plasticity in hippocampal dentate gyrus area: an in vivo study in anesthetized rats. *Biol Trace Elem Res* 2011;**143**:1616-1628.

9. Zhang L, Bai R, Li B, Ge C, Du J, Liu Y et al. Rutile TiO_2 particles exert size and surface coating dependent retention and lesions on the murine brain. *Toxicol Lett* 2011;**207**:73-81.

10. De Astis S, Corradini I, Morini R, Rodighiero S, Tomasoni R, Lenardi C et al. Nanostructured TiO2 surfaces promote polarized activation of microglia, but not astrocytes, toward a proinflammatory profile. *Nanoscale* 2013;**5**:10963-10974.

11. Ze Y, Sheng L, Zhao X, Hong J, Ze X, Yu X et al. TiO2 nanoparticles induced hippocampal neuroinflammation in mice. *PLoS One* 2014;**9**:e92230.

12. Hanani M. Satellite glial cells in sensory ganglia: from form to function. *Brain Res Brain Res Rev* 2005;**48**:457-476.

13. Pannese E. The structure of the perineuronal sheath of satellite glial cells (SGCs) in sensory ganglia. *Neuron Glia Biol* 2010;**6**:3-10.

14. Smijs TG, Bouwstra JA. Focus on skin as a possible port of entry for solid nanoparticles and the toxicological impact. *J Biomed Nanotechnol* 2010;**6**:469-484.

15. Wu J, Liu W, Xue C, Zhou S, Lan F, Bi L et al. Toxicity and penetration of TiO2 nanoparticles in hairless mice and porcine skin after subchronic dermal exposure. *Toxicol Lett* 2009;**191**:1-8.

16. Mühlfeld C, Geiser M, Kapp N, Gehr P, Rothen-Rutishauser B. Re-evaluation of pulmonary titanium dioxide nanoparticle distribution using the "relative deposition index": Evidence for clearance through microvasculature. *Part Fibre Toxicol* 2007;**4**:7.

17. Chen J, Dong X, Zhao J, Tang G. In vivo acute toxicity of titanium dioxide nanoparticles to mice after intraperitioneal injection. *J Appl Toxicol* 2009;**29**:330-337.

18. Bacquin A, Pouvelle C, Siaud N, Perderiset M, Salomé-Desnoulez S, Tellier-Lebegue C et al. The helicase FBH1 is tightly regulated by PCNA via CRL4(Cdt2)-mediated proteolysis in human cells. *Nucleic Acids Res* 2013;**41**:6501-6513.

19. Rajh T, Dimitrijevic NM, Rozhkova EA. Titanium dioxide nanoparticles in advanced imaging and nanotherapeutics. *Methods Mol Biol* 2011;**726**:63-75.

20. Jacobs JM, Macfarlane RM, Cavanagh JB. Vascular leakage in the dorsal root ganglia of the rat, studied with horseradish peroxidase. *J Neurol Sci* 1976;**29**:95-107.

21. Wu HH, Bellmunt E, Scheib JL, Venegas V, Burkert C, Reichardt LF et al. Glial precursors clear sensory neuron corpses during development via Jedi-1, an engulfment receptor. *Nat Neurosci* 2009;**12**:1534-1541.

22. Bolis V, Busco C, Ciarletta M, Distasi C, Erriquez J, Fenoglio I et al. Hydrophilic/hydrophobic features of TiO2 nanoparticles as a function of crystal phase, surface area and coating, in relation to their potential toxicity in peripheral nervous system. *J Colloid Interface Sci* 2012;**369**:28-39.

23. Erriquez J, Bernascone S, Ciarletta M, Filigheddu N, Graziani A, Distasi C. Calcium signals activated by ghrelin and D-Lys(3)-GHRP-6 ghrelin antagonist in developing dorsal root ganglion glial cells. *Cell Calcium* 2009;**46**:197-208.

24. Hubert T, Grimal S, Ratzinger S, Mechaly I, Grassel S, Fichard-Carroll A. Collagen XVI is a neural component of the developing and regenerating dorsal root ganglia extracellular matrix. *Matrix Biol* 2007;**26**:206-210.

25. ZHANG N-C, GAO Y-HW, Chui MingLIU, Ying-Liang. Preparation and Application of Fluorescein Isothiocyanate Fluorophore Nano-composites Chinese *Journal of Analytical Chemistry* 2010;**38**:p. 202–206.

26. Scherbart AM, Langer J, Bushmelev A, van Berlo D, Haberzettl P, van Schooten FJ et al. Contrasting macrophage activation by fine and ultrafine titanium dioxide particles is associated with different uptake mechanisms. *Part Fibre Toxicol* 2011;**8**:31.

27. Gerloff K, Fenoglio I, Carella E, Kolling J, Albrecht C, Boots AW et al. Distinctive toxicity of TiO2 rutile/anatase mixed phase nanoparticles on Caco-2 cells. *Chem Res Toxicol* 2012;**25**:646-655.

28. De Vos KJ, Grierson AJ, Ackerley S, Miller CC. Role of axonal transport in neurodegenerative diseases. *Annu Rev Neurosci* 2008;**31**:151-173.

29. Perlson E, Maday S, Fu MM, Moughamian AJ, Holzbaur EL. Retrograde axonal transport: pathways to cell death? *Trends Neurosci* 2010;**33**:335-344.

30. Bowen S, Ateh DD, Deinhardt K, Bird MM, Price KM, Baker CS et al. The phagocytic capacity of neurones. *Eur J Neurosci* 2007;**25**:2947-2955.

31. Ohara PT, Vit JP, Bhargava A, Romero M, Sundberg C, Charles AC et al. Gliopathic pain: when satellite glial cells go bad. *Neuroscientist* 2009;**15**:450-463.

32. Liu S, Xu L, Zhang T, Ren G, Yang Z. Oxidative stress and apoptosis induced by nanosized titanium dioxide in PC12 cells. *Toxicology* 2010;**267**:172-177.

33. Sohaebuddin SK, Thevenot PT, Baker D, Eaton JW, Tang L. Nanomaterial cytotoxicity is composition, size, and cell type dependent. *Part Fibre Toxicol* 2010;**7**:22.

34. Kang SJ, Kim BM, Lee YJ, Hong SH, Chung HW. Titanium dioxide nanoparticles induce apoptosis through the JNK/p38-caspase-8-Bid pathway in phytohemagglutinin-stimulated human lymphocytes. *Biochem Biophys Res Commun* 2009;**386**:682-687.

35. Braydich-Stolle LK, Schaeublin NM, Murdock RC, Jiang J, Biswas P, Schlager JJ et al. Crystal structure mediates mode of cell death in TiO2 nanotoxicity *Journal of Nanoparticle Research*; 2009;**11**:1361-1374

36. Chan J, Ying T, Guang YF, Lin LX, Kai T, Fang ZY et al. In vitro toxicity evaluation of 25-nm anatase TiO2 nanoparticles in immortalized keratinocyte cells. *Biol Trace Elem Res* 2011;**144**:183-196.

37. Jin C, Tang Y, Yang FG, Li XL, Xu S, Fan XY et al. Cellular toxicity of TiO2 nanoparticles in anatase and rutile crystal phase. *Biol Trace Elem Res* 2011;**141**:3-15.

38. Wu J, Sun J, Xue Y. Involvement of JNK and P53 activation in G2/M cell cycle arrest and apoptosis induced by titanium dioxide nanoparticles in neuron cells. *Toxicol Lett* 2010;**199**:269-276.

39. Shi Y, Wang F, He J, Yadav S, Wang H. Titanium dioxide nanoparticles cause apoptosis in BEAS-2B cells through the caspase 8/t-Bid-independent mitochondrial pathway. *Toxicol Lett* 2010;**196**:21-27.

40. Hussain S, Thomassen LC, Ferecatu I, Borot MC, Andreau K, Martens JA et al. Carbon black and titanium dioxide nanoparticles elicit distinct apoptotic pathways in bronchial epithelial cells. *Part Fibre Toxicol* 2010;**7**:10.

41. Liu S, Yang Z. Evaluation of the effect of acute and subacute exposure to TiO_2 nanoparticles on oxidative stress. *Methods Mol Biol* 2013;**1028**:135-145.

42. Shichiri M. The role of lipid peroxidation in neurological disorders. *J Clin Biochem Nutr* 2014;**54**:151-160.

43. Sayes CM, Wahi R, Kurian PA, Liu Y, West JL, Ausman KD et al. Correlating nanoscale titania structure with toxicity: a cytotoxicity and inflammatory response study with human dermal fibroblasts and human lung epithelial cells. *Toxicol Sci* 2006;**92**:174-185.

44. Jiang J, Oberdörster G, Elder A, Gelein R, Mercer P, Biswas P. Does Nanoparticle Activity Depend upon Size and Crystal Phase? *Nanotoxicology* 2008;**2**:33-42.

45. Fenoglio I, Ponti J, Alloa E, Ghiazza M, Corazzari I, Capomaccio R et al. Singlet oxygen plays a key role in the toxicity and DNA damage caused by nanometric TiO2 in human keratinocytes. *Nanoscale* 2013;**5**:6567-6576.

46. Fenoglio I, Greco G, Livraghi S, Fubini B. Non-UV-induced radical reactions at the surface of TiO2 nanoparticles that may trigger toxic responses. *Chemistry* 2009;**15**:4614-4621.

47. Oberdörster G, Oberdörster E, Oberdörster J. Nanotoxicology: an emerging discipline evolving from studies of ultrafine particles. *Environ Health Perspect* 2005;**113**:823-839.

48. Singh S, Shi T, Duffin R, Albrecht C, van Berlo D, Höhr D et al. Endocytosis, oxidative stress and IL-8 expression in human lung epithelial cells upon treatment with fine and ultrafine TiO2: role of

the specific surface area and of surface methylation of the particles. *Toxicol Appl Pharmacol* 2007;**222**:141-151.

49. Uttara B, Singh AV, Zamboni P, Mahajan RT. Oxidative stress and neurodegenerative diseases: a review of upstream and downstream antioxidant therapeutic options. *Curr Neuropharmacol* 2009;**7**:65-74.

50. Morfini G, Pigino G, Opalach K, Serulle Y, Moreira JE, Sugimori M et al. 1-Methyl-4-phenylpyridinium affects fast axonal transport by activation of caspase and protein kinase C. *Proc Natl Acad Sci U S A* 2007;**104**:2442-2447.

CIT1A Shi et al. Particle and Fibre Toxicology 2013, 10:15

CIT1B Tissue distribution and elimination after oral and intravenous administration of different titanium dioxide nanoparticles in rats.Geraets L, Oomen AG, Krystek P, Jacobsen NR, Wallin H, Laurentie M, Verharen HW, Brandon EF, de Jong WH. Part Fibre Toxicol. 2014 Jul 3;11:30. doi: 10.1186/1743-8977-11-30.),

CIT1C Part Fibre Toxicol. 2010 Jun 14;7:16. doi: 10.1186/1743-8977-7-16. Effects of prenatal exposure to surface-coated nanosized titanium dioxide (UV-Titan). A study in mice. Hougaard KS1, Jackson P, Jensen KA, Sloth JJ, Löschner K, Larsen EH, Birkedal RK, Vibenholt A, Boisen AM, Wallin H, Vogel U.

CIT1D Yang Li, Yi Zhang and Bing Yan Nanotoxicity Overview: Nano-Threat to Susceptible Populations Int. J. Mol. Sci. 2014, 15, 3671-3697; doi:10.3390/ijms15033671

CIT2A A. de la Mano et al. / Cytokine 37 (2007) 128–137

CIT2B Stuart M. Allan, Pippa J. Tyrrell & Nancy J. Rothwell Interleukin-1 and neuronal injury *Nature Reviews Immunology* **5**, 629-640 (August 2005) | doi:10.1038/nri1664

Figure legends

Figure 1. Appearance of primary cultures of DRG of chicken embryos alone (a) and when incubated with 0.5 μg/ml (b) 5.0 μg/ml (c) of TiO_2-A/R-NPs dispersions.

Figure 2. Apoptosis induced by TiO_2-A/R-NPs on DRG cells measured by TUNEL assay. (a) Representative images of DRG cells doubly stained with propidium iodide (left column) and TUNEL (middle column) in different conditions (Control, 0.5 μg/ml or 5.0 μg/ml of TiO_2-A/R-NPs) . Bar = 20 μm. b) Bar-graph showing the percentages of TUNEL-positive cells after treatment with two doses of TiO2-A/R-NPs. * $p < 0.05$; ** $p < 0.01$.

Figure 3. Double DAPI-Nissl DRG cells staining. a) DAPI labeled DRG nuclei; b) Nissl labeled DRG cells; c) merge of a and b showing a neuron with a Nissl-positive cytoplasm, an eccentric nucleus with two nucleoli and SGCs nuclei with Nissl-positive clumps. d) The arrow indicate a fragmented nucleus of a neuron. e) The arrow indicate a fragmented nucleus of a glial cell. The mean percentages of apoptotic DRG cells are represented in bar-graphs: percentage of all apoptotic DRG cells (f), of apoptotic glial cells (g) and of apoptotic neurons (h), respectively, in control conditions (CTRL), after incubation with 0.5 μg/ml of TiO_2-A/R-NPs and after incubation with 5.0 μg/ml of TiO_2-A/R-NPs; Bar = 10 μm. ANOVA, ** and ++ $p < 0.01$; * $p < 0.05$.

Figure 4. Intracellular localization of TiO_2-A/R-NPs in DRG. a) A neuron and its neurites after 2 hours of incubation with FITC-TiO_2-A/R-NPs: a_2) localization of green FITC-TiO_2-A/R-NPs (TiO_2-A/R) along neurites and in cell body; a_3) LysoTracker Red positive organelles along neurites and in cell body; a_4) a_2 and a_3 merge shows colocalization (yellow areas) of internalized FITC-TiO_2-A/R-NPs and organelles. b) SGCs after 2 hours of incubation with FITC-TiO_2-A/R NPs: b_2) localization of

green FITC-TiO_2-A/R-NPs in the cell body; b_3) LysoTracker Red positive organelles in cell body; b_4) b_2 and b_3 merge shows colocalization (yellow areas) of internalized FITC-TiO_2-A/R-NPs and organelles. c_{1-4}) Z stack of merged images of a neuron and its neurite after 24 hours of incubation with FITC-TiO_2-A/R-NPs and LysoTracker Red; d_{1-4}) Z stack of merged images of a neuron and its neurite after 24 hours of incubation with FITC-TiO_2-A/R-NPs and MitoTracker Orange CMTMRos . e_{1-5}) Z stack of merged images of a glial cell after 24 hours of incubation with FITC-TiO_2-A/R-NPs and MitoTracker Orange CMTMRos.

Figure 5. Effects of TiO_2-NPs on retrograde axonal transport. Example of vesicle tracking: orange line in (b) is the trajectory traced by the vesicle selected in the yellow square along the neurite of the DRG neuron shown in (a). Mean speed of retrograde axonal vesicles in untreated neurons and in neurons incubated with FITC-TiO_2-A/R (c) and FITC-TiO_2-R (f). Histograms showing the distributions of the speed obtained in the in control condition (d, g) and in the presence of FITC-TiO_2-A/R (e) or FITC-TiO_2-R (h).

Figure 6. Effects of TiO_2-NPs on ROS generation and IL-1β expression. a) Representative images of DRG cells doubly stained with DAPI and CellROX in different conditions (top); confocal reflection images (middle) of the same fields; merged images (bottom). Bar = 10 μm. b) Bar-graph showing the percentages of CellROX-positive cells after the different treatments. ANOVA, ** $p < 0.01$ c) IL-1β mRNA expression, normalized to that of β-actin in control cells and in cells treated for 24 hours with 5 μM of TiO2-A/R-NPs.

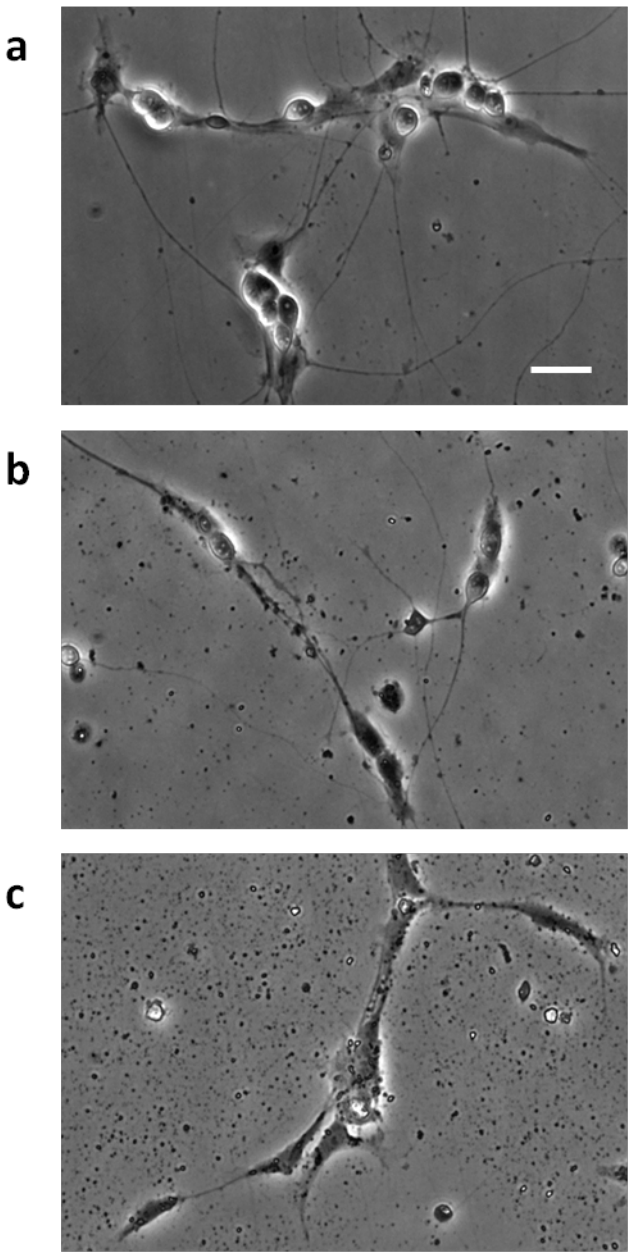

Figure 1

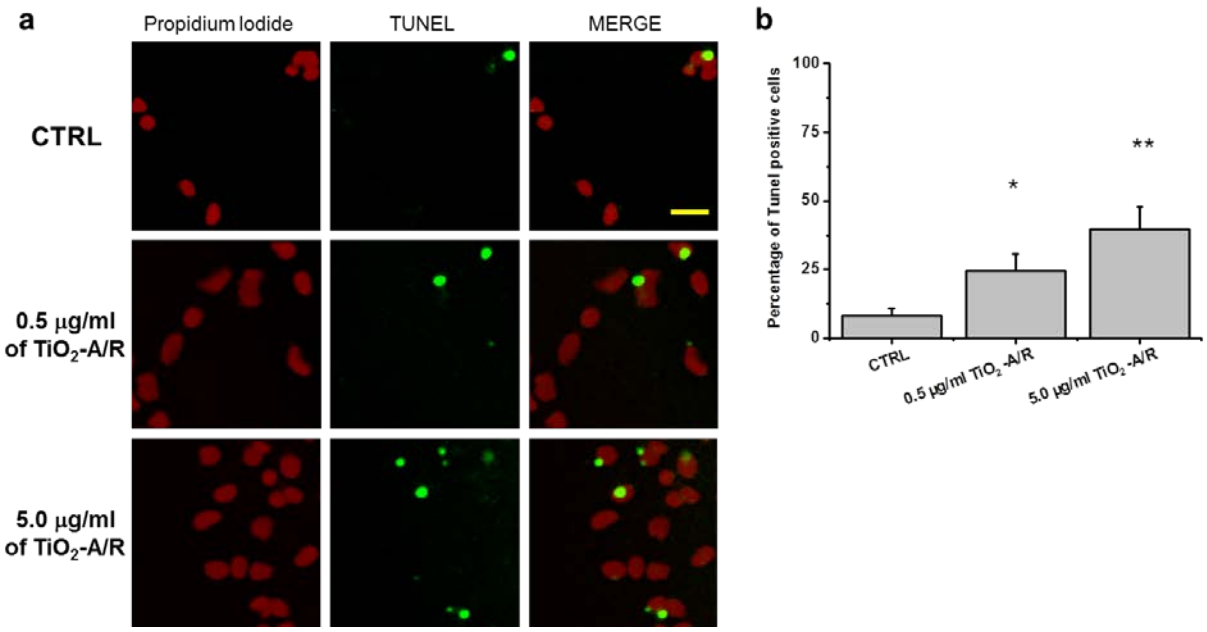
a
Propidium Iodide
TUNEL
MERGE
CTRL
0.5 μg/ml of TiO2-A/R
5.0 μg/ml of TiO2-A/R
b
Percentage of Tunel positive cells
100
75
50
25
0
*
**
CTRL
0.5 μg/ml TiO2 -A/R
5.0 μg/ml TiO2 -A/R

Figure 2

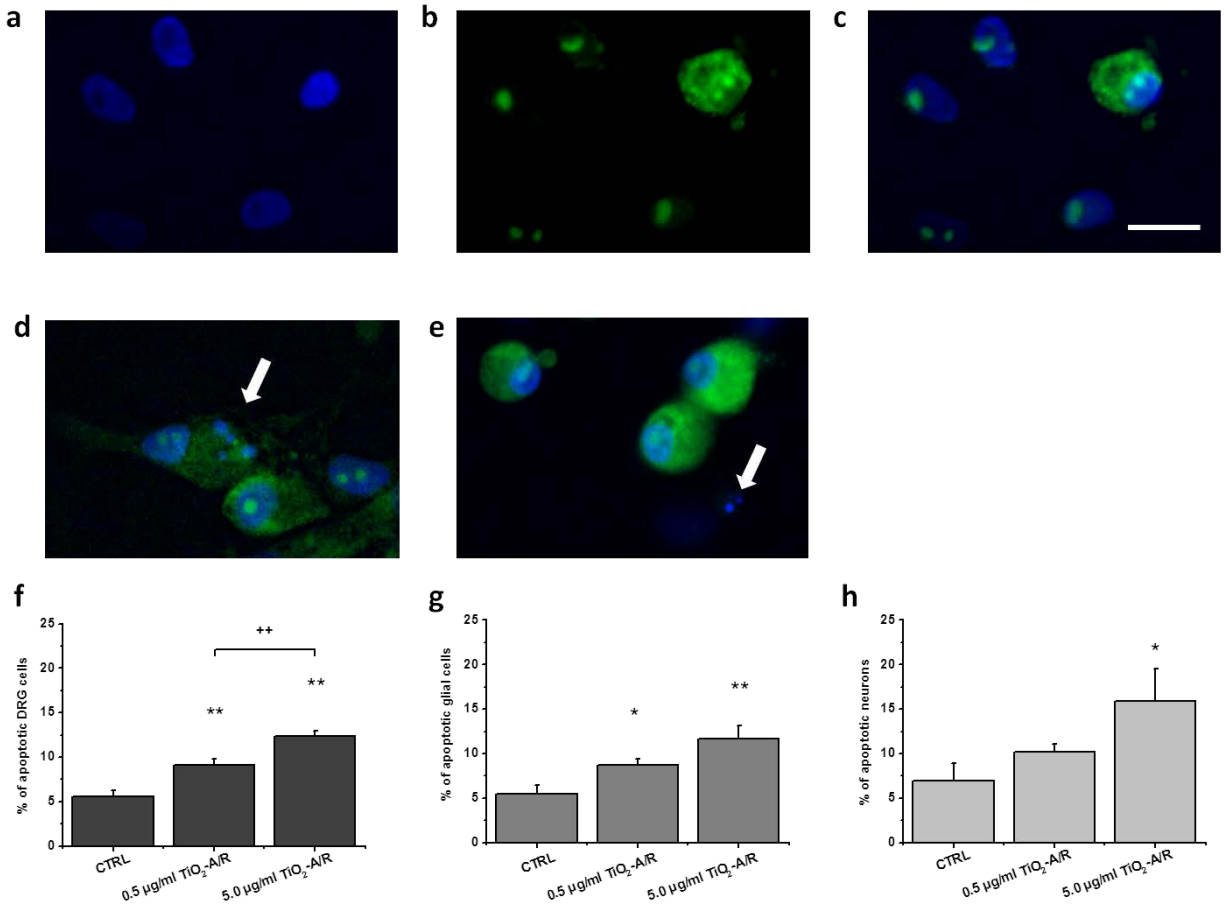
a
b
c
d
e
f
g
h
% of apoptotic DRG cells
% of apoptotic glial cells
% of apoptotic neurons
CTRL
0.5 µg/ml TiO2-A/R
5.0 µg/ml TiO2-A/R
++
**
*

Figure 3

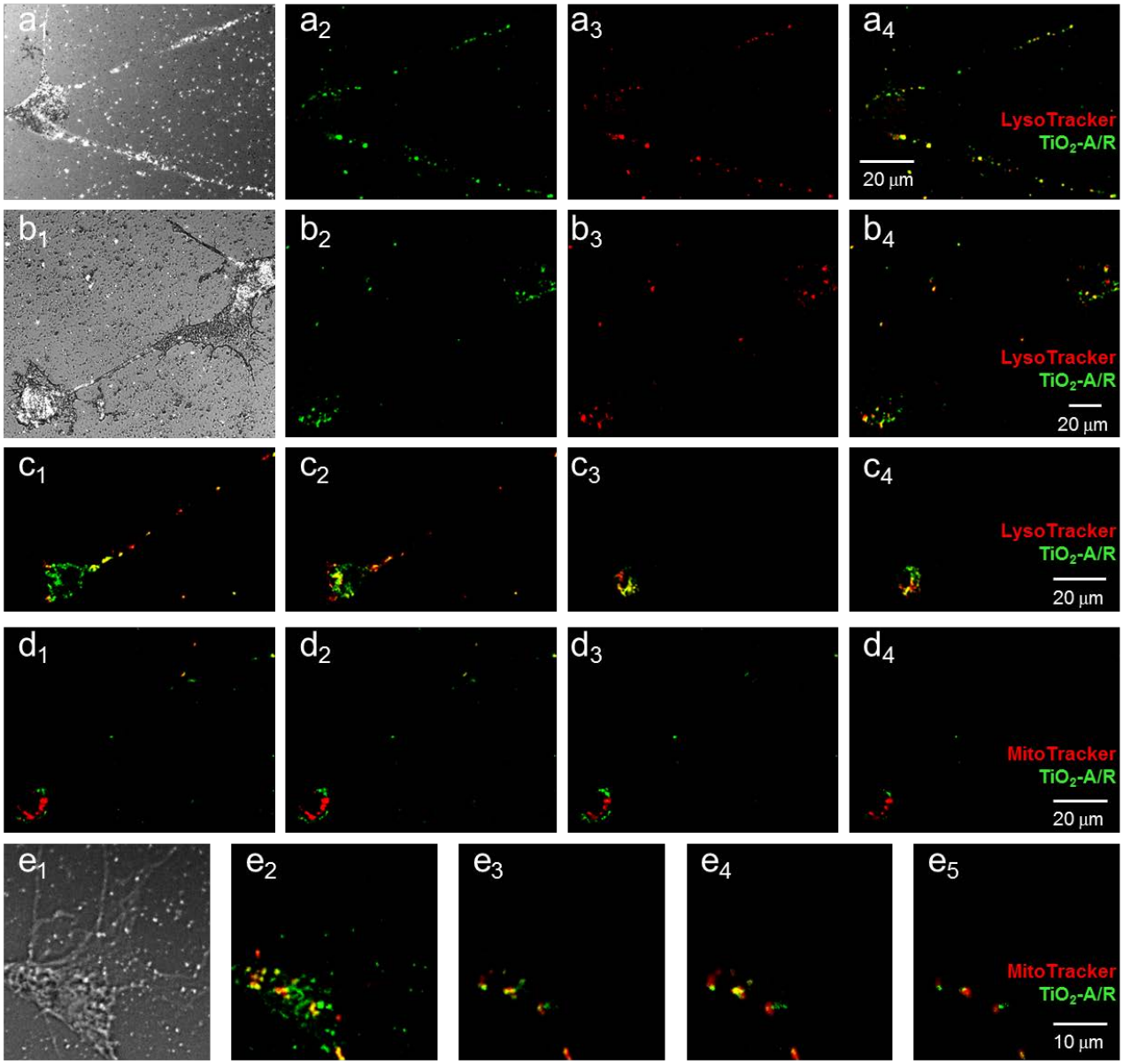
a1
a2
a3
a4
LysoTracker
TiO2-A/R
20 μm
b1
b2
b3
b4
LysoTracker
TiO2-A/R
20 μm
c1
c2
c3
c4
LysoTracker
TiO2-A/R
20 μm
d1
d2
d3
d4
MitoTracker
TiO2-A/R
20 μm
e1
e2
e3
e4
e5
MitoTracker
TiO2-A/R
10 μm

Figure 4

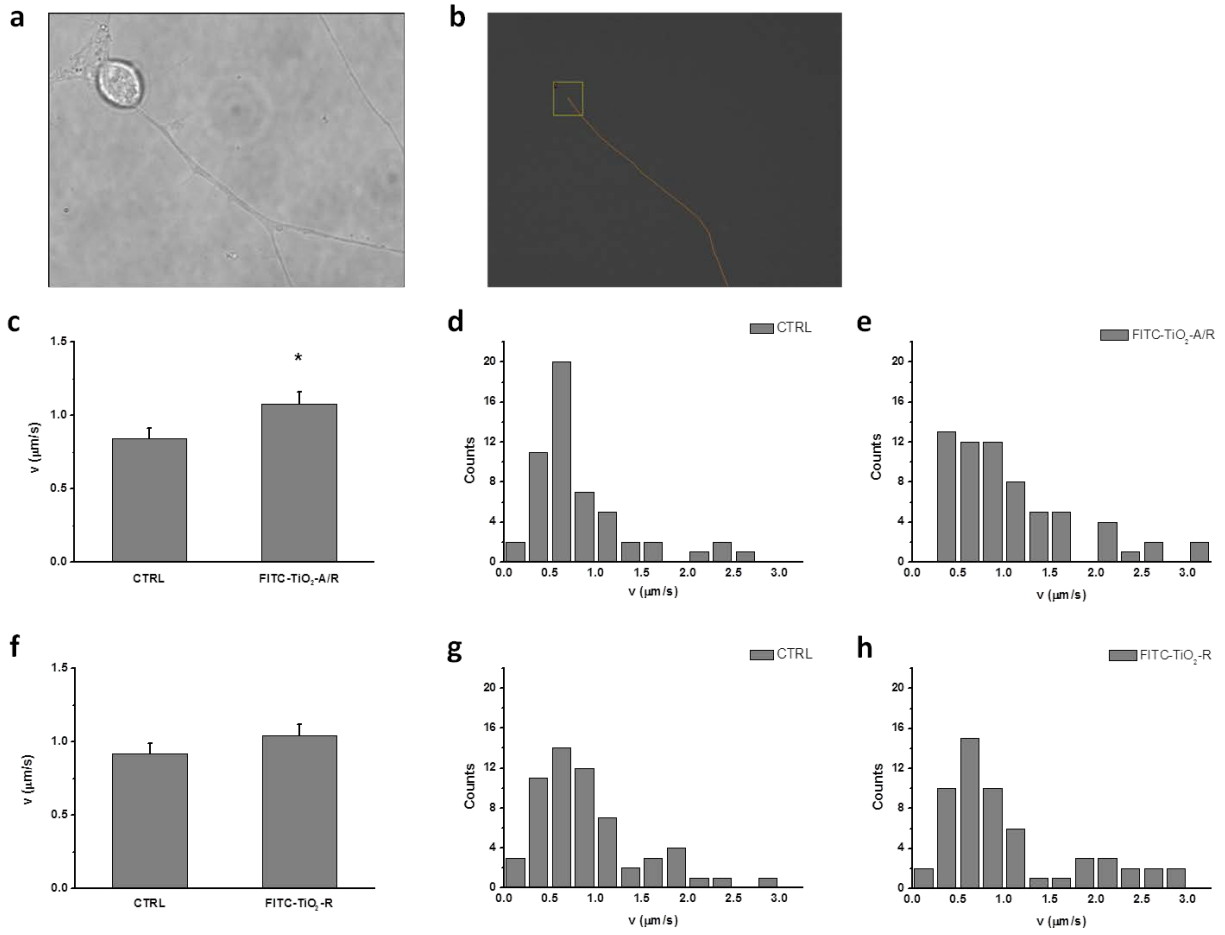
a
b
c
v (μm/s)
*
CTRL
FITC-TiO2-A/R
d
CTRL
Counts
v (μm/s)
e
FITC-TiO2-A/R
Counts
v (μm/s)
f
v (μm/s)
CTRL
FITC-TiO2-R
g
CTRL
Counts
v (μm/s)
h
FITC-TiO2-R
Counts
v (μm/s)

Figure 5

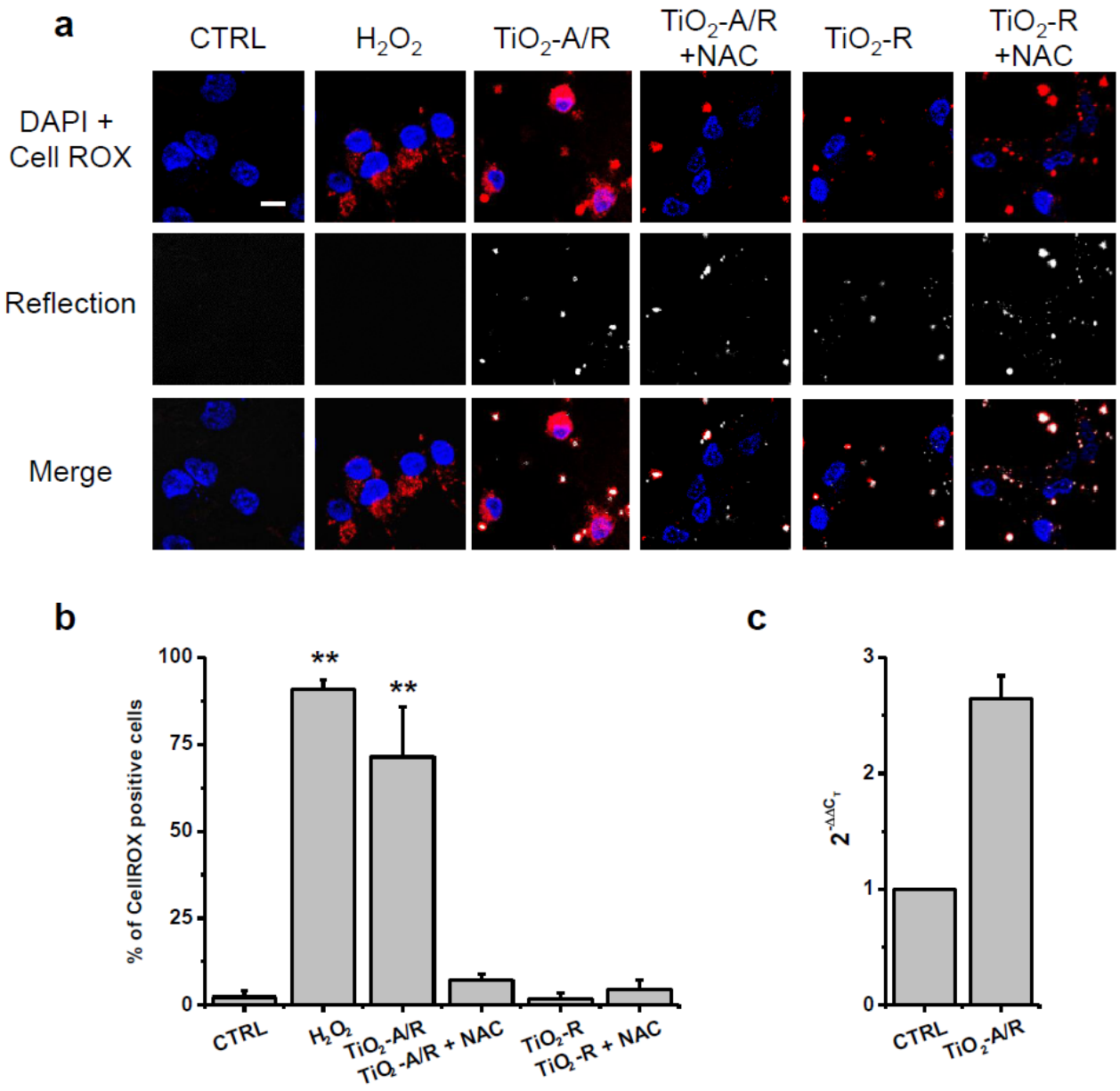
a
CTRL
H2O2
TiO2-A/R
TiO2-A/R +NAC
TiO2-R
TiO2-R +NAC
DAPI + Cell ROX
Reflection
Merge
b
% of CellROX positive cells
100
75
50
25
0
**
**
CTRL
H2O2
TiO2-A/R
TiO2-A/R + NAC
TiO2-R
TiO2-R + NAC
c
2-ΔΔCT
3
2
1
0
CTRL
TiO2-A/R

Figure 6

Supplementary Material

Characterization of the label.

To characterize the structure of the fluorescent label, the solvent was evaporated by argon bubbling, thus reducing the volume considerably. The addition of diethyl ether gave precipitation of a yellow orange powder that could be isolated by centrifugation and washed 3 times with 10 ml of diethyl ether. This solid material was rapidly filtered, dried and dissolved in CD_3OH + 1 drop of NaOD for the NMR proton analysis. The NMR spectrum is in general agreement with the proposed structure apart from a slightly scarce integration of ethoxy groups of the silane, that suggest high reactivity of the product in a basic medium, as known for alkoxy-silanes.

NMR (CD3OD/NaOD, 200 MHx): δ (ppm): 7.69 (s, 1H, Ar); 7.30 (m, 3H, Ar), 7.04 (d, 1H, Ar), 6.51 (m, 4H, Ar), 3.61 (q, 6H, CH_2CH_3), 3.44 (m, 2H, $NHCH_2CH_2CH_2$), 2.57 (t, 1H, $NHCH_2$); 1.76 (broad, 2H, $CH_2CH_2CH_2$), 1.18 (t, 9H, CH_2CH_3), 0.62 (t, 2H, CH_2Si).

MS-ESI(-) (m/z): 609.18.

Table S1. Properties of the TiO_2 NPs used in this study

Sample	Polymorph	Crystallites size (nm)	Specific surface area (m^2/g)
TiO_2-A	Anatase	11 ± 1	72
TiO_2-R	Rutile	31 ± 2	39
TiO_2-A/R	Anatase 80%; Rutile 20%	30 ± 4 (A); 50 ± 6 (R)	53

Table S2. Effect of labeling on the surface properties of nanoparticles

Sample	Zeta potential (mV) in culture medium		Hydrodynamic diameter in culture medium	
	pristine	FITC-labeled	Pristine	FITC-labeled
TiO_2-A	-20 ± 2	-18 ± 2	306 ± 19 (PDI 0.4)	300 ± 10 (PDI 0.5)
TiO_2-R	-15 ± 1	-15 ± 3	206 ± 7 (PDI 0.4)	211 ± 11 (PDI 0.5)
TiO_2-A/R	-15 ± 1	-16 ± 2	256 ± 9 (PDI 0.4)	212 ± 5 (PDI 0.4)

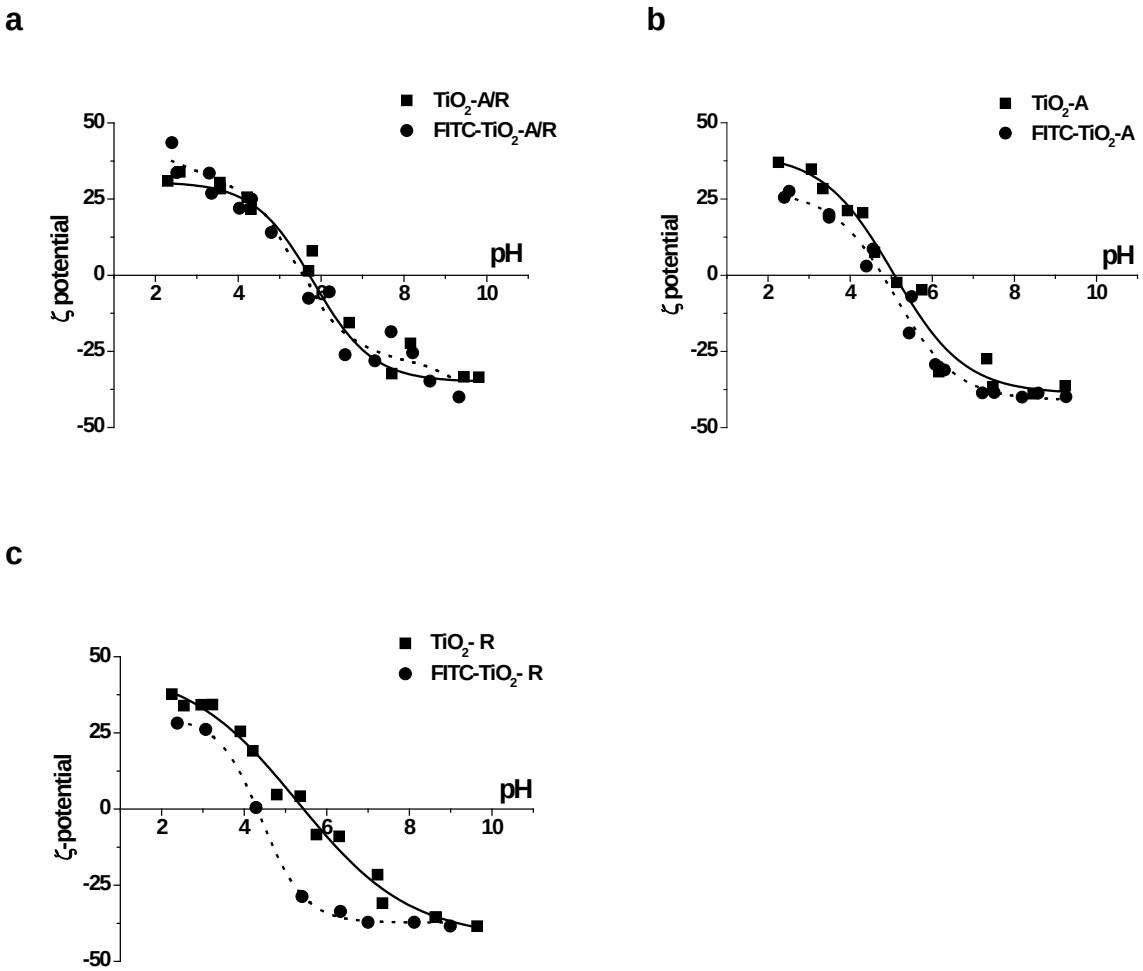

Figure S1. ζ potential as function of pH of FITC-labelled TiO_2 NPs (solid lines) versus pristine TiO_2 NPs (dot lines) suspended in NaCl 1 mM, 5 µg/ml.

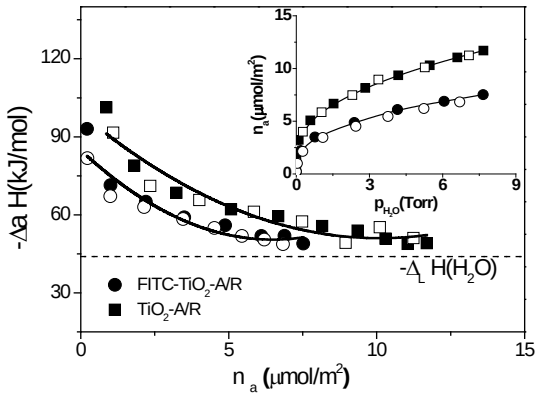

Figure S2. Adsorption enthalpy vs water uptake at T = 30 °C on TiO_2-A/R (square) and FITC-TiO_2-A/R (round) nanoparticles. In the inset the uptake of water molecules vs the equilibrium pressure. All samples were preliminary outgassed overnight at T = 30 °C, residual pressure $p \leq 10^{-4}$ Torr. The dashed line indicates the latent enthalpy of liquefaction of water $-\Delta_L$ = 44 kJ/mol.

Figure S3. Bar-graphs showing the percentages of TUNEL-positive DRG cells after treatment with two doses of TiO_2-R NPs (a) and of TiO_2-A NPs. Only TiO_2-A NPs induced apoptosis in DRG cells in a dose dependent manner. ** $p < 0.01$.

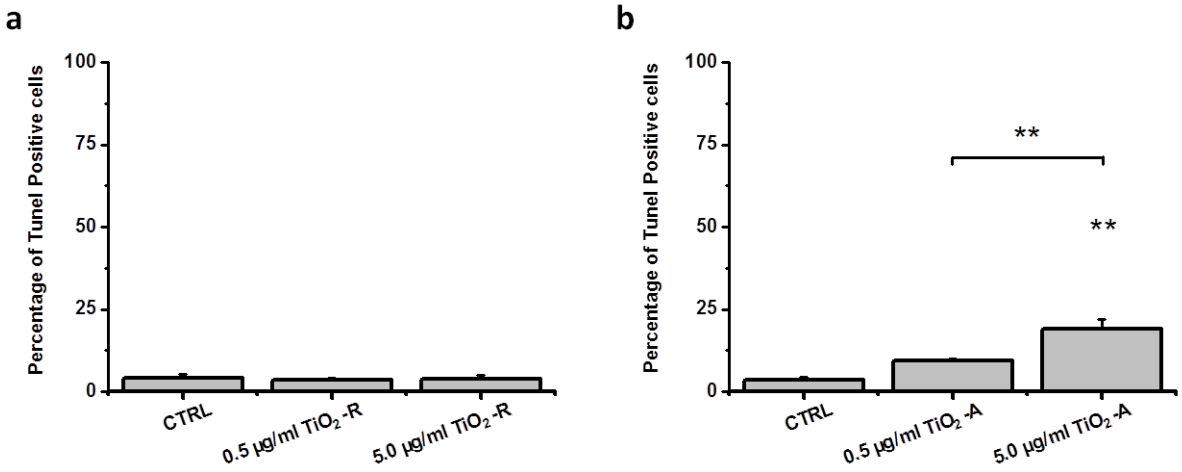

Figure S4. Intracellular localization of TiO_2-NPs in DRG cells. Z stack of merged images of a glial cells (G) and neuron (N) after 24 hours of incubation with FITC-TiO_2-A NPs (a) or FITC-TiO_2-R NPs (b) plus LysoTracker Red and after 24 hours of incubation with FITC-TiO_2-A NPs (a) or FITC-TiO_2-R NPs (b) plus MitoTracker Orange. Arrowheads highlight some double-positive vesicles along neurites. The localization profiles of FITC-TiO_2-A NPs and FITC-TiO_2-R NPs are comparable to the ones observed for FITC-TiO_2-A/R NPs.